Supplementary Materials for

Linking a mutation to survival in wild mice

Rowan D. H. Barrett*†, Stefan Laurent†, Ricardo Mallarino†, Susanne P. Pfeifer, Charles C. Y. Xu, Matthieu Foll, Kazumasa Wakamatsu, Jonathan S. Duke-Cohan, Jeffrey D. Jensen, Hopi E. Hoekstra*

*Corresponding author. Email: rowan.barrett@mcgill.ca (R.D.H.B.); hoekstra@oeb.harvard.edu (H.E.H.)
†These authors contributed equally to this work.

Published 1 February 2019, *Science* **363**, 499 (2019)
DOI: 10.1126/science.aav3824

This PDF file includes:

Materials and Methods

Enclosure construction and colonization

In May and June 2011, we constructed eight enclosures that contain 20,000 m^2 of habitat: four on a light-substrate site on the Sand Hills (the 'light site'; 42°35'13.44"N, 100°54'27.64"W) and four on a dark-substrate site off the Sand Hills (the 'dark site'; 42°54'5.27"N, 100°30'32.30"W). Each enclosure is 25 m x 25 m with steel plate walls (1.5 m by 3 m plates of 24-guage galvanized steel) buried 0.75 m into the ground. Following a previous study (*44*), we first trenched the perimeter of each enclosure to a depth of 0.75 m using a mechanical trencher equipped with a 15cm blade. We then buried steel posts (3.8 by 3.8 cm, 2.1 mm thick, and 2 m long) into the trench at 3 m intervals, allowing 1 m to protrude above ground. These posts served as supports for the walls, which we attached using self-tapping sheet metal screws. To extend the height of the walls to 1.8 m, steel posts (3.2 by 3.2 cm, 2.1 mm thick, cut to 1.2 m sections) were inserted 30 cm into the original support posts and secured using metal screws. We then attached chicken wire fencing (0.9 m high) to the extension posts with bailing wire to help exclude large mammals. Finally, we dug holes around the base of each post and filled with concrete for additional support. We removed native small mammals from each enclosure through repeated rounds of trapping using Sherman live traps.

Between June and October 2011, we sampled 481 mice using Sherman live traps from six locations within 50 km of each other (3 on light Sand Hills habitat and 3 on dark habitat, see table S8 for specific sampling locations; mice were collected under the Nebraska Game and Parks Commission Scientific and Educational Permit 901). We introduced between 75-100 of these mice to each of 6 of the 8 enclosures (3 at each site), with half coming from each habitat type. Prior to introduction, we anesthetized each mouse and recorded sex, age, length, weight, and pigmentation phenotype (see below). We did not detect significant differences in any non-pigment related traits between mice captured on light versus dark habitat. To allow for individual identification, we marked the ears and injected a small radio ID-tag between the scapula of each mouse. To collect DNA, we took a 1-mm diameter tail tip, which was preserved in ethanol.

Coat-color variation in experimental populations

To measure pigmentation among the experimental populations of deer mice, we used a spectrophotometer to measure reflectance of each mouse at 9 locations across the body (3 measurements along the dorsum, flank, and ventrum), as described previously (*13*). We then used Color Analysis Programs v1.05 (*45*) to process the raw SpectraSuite files and extracted 7 color summary statistics. We computed averages for each of these summary statistics for each of the body regions (dorsum, flank, ventrum), resulting in a total of 21 color variables for each mouse. After normal quartile transformation on each variable, we performed principle components analysis (PCA). After examining the scree plot, we selected the first 5 principal components (PCs), which together accounted for 84% of the variation in the data. Because factor loadings were not easily interpretable in the unrotated data, we performed a varimax rotation on the first 5 PCs (*46*). Based on their loadings, the top 5 PCs corresponded to dorsal/flank brightness and contrast, dorsal/flank hue, ventral chroma and hue, ventral brightness and contrast, and dorsal/flank chroma and hue. For simplicity, we refer to these PCs in the main text as dorsal brightness, dorsal hue, ventral chroma, ventral brightness, and dorsal chroma; all traits were normally distributed. Higher values of each trait correspond to lighter phenotypes.

Color pattern variation in experimental populations

We measured two aspects of color pattern: dorsal-ventral boundary and tail pattern. We took digital images of each mouse using a Canon EOS Rebel T3i (Canon U.S.A., Lake Success, NY) with a Sigma 18-250mm lens (Sigma U.S.A., Ronkonkoma, NY) and a X-Rite ColorChecker Passport (X-Rite, Grand Rapids, MI). We imported tiff files into ImageJ and outlined the dorsum (colored portions of the dorsum, with legs and tail excluded) and body (outlined entire mouse, legs and tail excluded). Dorsal-ventral boundary was calculated as (body-dorsum)/body, followed by a normal quartile transformation. We used the following qualitative scores for tail pattern: 0 = no colored portion, 1 = basal portion of tail is colored, 2 = colored portion extends to approximately half the length of the tail, 3 = intermittent color throughout full length of tail, 4 = full coloration of tail, following previous work (*47*).

Population sampling in the enclosures over time

Following the introduction of mice to the enclosures, we conducted 5 sampling trips (August 2011, October 2011, December 2011, April 2012, August 2012) to trap mice in the enclosures and determine survivorship of individuals in each population (individual identities were verified by use of implanted radio tags and a handheld reader). We used 50 traps per enclosure and conducted up to 40 trapping sessions in each enclosure each trip. We filled pairs of enclosures sequentially (approximately equal numbers of mice from light and dark habitat were added to one light and one dark enclosure each day). While the specific time periods used in our selection analyses (see below) vary among pairs of enclosures, the absolute period of time that each population was subjected to selection was similar. In our selection analyses, we assume that a mouse not captured during a trip has died. To justify this assumption, we estimated our recapture rate and also tested for an association between pigmentation and likelihood of capture (such an association, if it existed, could potentially bias our estimates of selection). To do this, we used a Cormack-Jolly-Seber (CJS) model (*48*, *49*) to analyze capture-recapture data across multiple sampling trips. We chose this model to estimate rates of capture and survival because it is easily tailored to our experimental design, in which all individuals are initially marked and released (*50*). Our model included main effects of pigmentation trait and soil treatment, as well as an interaction between these two variables, as predictors on the rate of recapture. Our overall recapture rate was high (0.949; 95% BCI: 0.904, 0.979). Moreover, the 95% Bayesian credible intervals for the effect of pigmentation trait and the interaction effect between pigmentation trait and soil treatment on recapture all overlap zero. Thus, the small number of individuals that evade detection during our sampling are not a biased subset with respect to any of the experimental variables investigated here. Finally, we used CJS models to quantify the effects of soil treatment and either pigmentation trait or source habitat (along with interactions) on survival (table S2).

Measuring natural selection on pigmentation traits

We used selection analyses (*51*-*53*) to characterize the form, intensity, and direction of selection acting on all traits we had *a priori* reason to suspect as being important to survival (*13*, *14*) - that is, those traits found to be significantly different between mice captured on light versus dark habitat: dorsal brightness, dorsal chroma, ventral brightness, ventral chroma, and tail pattern. For all phenotypic analyses, we used only adult mice as coat color and pattern can change from juvenile to adult pelage, and color variation is low among juvenile mice (most juveniles are a consistent grey color). However, including juveniles in the analyses did not change the direction of selection for any trait.

For each enclosure, we estimated the fitness function relating survival (0 or 1) to the five traits using a generalized additive model (GAM) and the default settings in the function gam in the R

package MGCV version 1.8-12 (*54*). We then used the function gam.gradients in the R package GSG version 2 (*53*) to obtain directional and quadratic selection gradients. We evaluated the statistical uncertainty in the estimated selection gradients using 1000 bootstrap replicates. Following the first time period, there was sufficient mortality (Fig. 2, A and B) that population sizes were not large enough to fit a GAM to all phenotypic traits (there were more coefficients in the model than data), and thus we did not continue our selection analyses past the first re-sampling point.

The methods above identified dorsal brightness as the only trait with consistent evidence for selection across multiple enclosures. To visualize selection on this trait without *a priori* assumptions about the shape of the fitness function, we produced nonparametric fitness surfaces for each treatment (*52*, *55*). We generated predicted values and Bayesian standard errors for the cubic splines using a GAM in the function gam of the R package MGCV version 1.8-12 (*54*). Smoothing parameters were chosen from values that minimized the generalized cross-validation (GCV) scores. We then visualized fitness surfaces by plotting predicted values with 1 Bayesian standard error, using the inverse of the logit link function to obtain the original scale.

DNA sequencing library preparation

To prepare sequencing libraries, we used DNeasy kits (Qiagen, Germantown, MD) to extract DNA from tail samples. We then prepared genomic libraries following the SureSelect Target Enrichment Protocol v.1.0, with some modifications. In brief, 10-20 μg of each DNA sample was sheared to an average size of 200 base pairs (bp) using a Covaris ultrasonicator (Covaris Inc., Woburn, MA). Sheared DNA samples were purified with Agencourt AMPure XP beads (Beckman Coulter, Indianapolis, IN) and quantified using a Quant-iT dsDNA Assay Kit (ThermoFisher Scientific, Waltham, MA). We then performed end-repair and adenylation, using 50 μl ligations with Quick Ligase (New England Biolabs, Ipswich, MA) and paired-end adapter oligonucleotides manufactured by Integrated DNA Technologies (Coralville, IA). Each sample was assigned one of 48 5-bp barcodes. We pooled samples into equimolar sets of 9-12 and conducted size selection of a 280-bp band (+/- 50-bp) on a Pippin Prep with a 2% agarose gel cassette. We performed 12 cycles of PCR with Phusion High-Fidelity DNA Polymerase (NEB), following manufacturer guidelines. To permit additional multiplexing beyond that permitted by 48 barcodes, we also added one of 12 6-bp indices to each pool of 12 barcoded samples. Following amplification and AMPure purification, we assessed the quality and quantity of each pool (17 total; see below) with an Agilent 2200 TapeStation (Agilent Technologies, Santa Clara, CA) and a Qubit-BR dsDNA Assay Kit (Thermo Fisher Scientific, Waltham, MA).

DNA enrichment and sequencing

To enrich sample libraries for both the *Agouti* locus as well as randomly distributed genomic regions, we used a MYcroarray MYbaits capture array (MYcroarray, Ann Arbor, MI). In brief, this probe set includes the 185-kb region containing all known *Agouti* coding exons and regulatory elements (based on a *P. maniculatus Agouti* BAC clone (*56*)) and >1000 non-repetitive regions averaging 1.5-kb in length at random locations across the *P. maniculatus* genome. We enriched for regions of interest following the standard MYbaits v.2 protocol for hybridization, capture, and recovery. We then performed 14 cycles of PCR with Phusion High-Fidelity Polymerase and a final AMPure purification. We assessed final quantity and quality using a Qubit-HS dsDNA Assay Kit and Agilent 2200 TapeStation.

After enriching our libraries for regions of interest, we combined them into 17 pools and

sequenced across 10 lanes of 125-bp paired-end reads using an Illumina HiSeq2500 platform (Illumina, San Diego, CA). From the obtained read pairs, 94% could be confidently assigned to individual samples (i.e., excluding reads when either barcodes or indices were ambiguous and/or had low base qualities), resulting in an average read pair count of 2,674,111 per individual.

Sequence alignment

Following our previous approach (*15*), we first removed contaminants and low-quality nucleotides. Partially error-corrected, single-end reads were generated from each read pair using FLASH v.1.2.11 (*57*) and aligned to the repeat-masked *Peromyscus maniculatus bairdii* Pman_1.0 reference assembly (http://www.ncbi.nlm.nih.gov/assembly/GCF_000500345.1/). More than 98% of all reads mapped to the reference genome. Finally, we removed duplicates, conducted multiple sequence alignments, and adjusted base qualities.

Variant Calling and Filtering

Following (*15*), variants were called per individual, and diploid genotypes were jointly inferred per enclosure pair (*i.e.*, one 'light' and one 'dark' enclosure with n_1=203 individuals, and n_2=147, n_3=122). Post-genotyping, we excluded 10 individuals with more than 80% missing data and merged all enclosures into a pooled dataset. A principal component analysis (PCA) of the data revealed the presence of 16 outlier individuals that were then also excluded. We further restricted this pooled dataset to biallelic variants that were genotyped in at least 80% of individuals. In the absence of a validation dataset for this species, we applied stringent hard filter criteria to avoid false positives due to sequencing errors or alignment issues (see (*15*) for details). The final call set contained 2,442 variants for the *Agouti* scaffold and 53,507 for the genome-wide control dataset. We conducted analyses of single enclosures by sub-setting the pooled data with the appropriate list of individuals, such that the same set of variants could be compared across all soil colors and replicates.

Standardizing the SNP dataset across enclosures

For each treatment (soil color), we created a pooled dataset consisting of all SNPs present in the 3 enclosures. We applied a missing data filter to both pooled datasets independently. For each treatment, we removed individuals with more than 80% missing nucleotide sites. Among the remaining individuals, we removed sites with more than 20% missing data. Finally, we conducted enclosure-specific analyses by back-partitioning the pooled data such that the same set of SNPs could be compared among enclosures. We tested for differences in starting allele frequency between enclosures in each treatment using Kruskal-Wallis tests of minor allele frequencies (MAF < 0.1) and found no significant differences (light soil enclosures: $\chi = 0.898$, df = 2, P = 0.638; dark soil enclosures: $\chi = 0.211$, df = 2, P = 0.900). There were also no significant differences in allele frequency between mice caught from different source locations in either habitat type (light soil locations: $\chi = 0.020$, df = 2, P = 0.890; dark soil locations: $\chi = 2.745$, df = 2, P = 0.254)

Calculation of probabilities of genotype distributions in surviving individuals

At each SNP, we calculated the change in allele frequency between surviving mice at time point 1 and the initial populations. To test whether absolute allele frequency changes were larger in the light treatment (as expected due to the higher mortality), we used a Wilcoxon rank sum test. We chose a non-parametric test because the absolute frequency changes did not follow a normal distribution.

To test the null hypothesis that survival and genotype were independent, we calculated for every variant the probability that genotype frequencies in the survivors were the result of unbiased (neutral) sampling using the multivariate hypergeometric distribution. This distribution describes the probability of the observed genotype frequencies in the survivors, given that draws were made without replacement and that sampling occurred in a finite population. From this analysis, we obtained the number of sites with $P < 0.01$. To test whether this number was a consequence of conducting a large number of statistical tests, we next calculated the distribution of the number of sites with $P < 0.01$ expected under neutrality using a permutation approach. Finally, to test whether the number of significant sites could be inflated due to linkage, we calculated the null distribution of sites with $P < 0.01$ assuming a model with a single site under selection. In cases where the number of sites with $P < 0.01$ could not be accounted for by random sampling and multiple testing, we also calculated for each variant the probability of the observed genotype frequencies assuming biased sampling. For this we used the complementary multivariate Wallenius non-central hypergeometric distribution (*55*). This distribution generalizes the multivariate hypergeometric distribution by allowing the sampled features (genotypes, in this case) to be sampled with bias. Importantly, this distribution accounts for the situation when sampling occurs both sequentially and with bias.

To test for significant selection at each locus, we calculated the ratio of biased over unbiased probabilities. We obtained P values for this likelihood ratio using a chi-square distribution with 2 degrees of freedom and set the significance threshold to 0.05 after FDR correction. The R code implementing these analyses is available from https://github.com/laurentlab-mpipz/rsurvival. A detailed description of this statistical approach is provided in the Supplemental Text. We calculated F_{ST} and LD using vcftools (--hap-r2 option, version 0.1.15). The code for the visualization in Fig. 4C is modified from https://stackoverflow.com/questions/22278951/combining-violin-plot-with-box-plot.

Functional testing of the *Agouti* mutation using site-specific transgenesis

To explicitly test if the Serine deletion mutation (ΔSer) in *Agouti* exon 2 has a measurable effect on pigmentation, we used a recombinase mediated cassette exchange approach to insert the *Peromyscus* wildtype (WT) and ΔSer alleles into the *Mus* C57BL/6, a strain that contains a knockout *Agouti* mutation.

Plasmids: To construct site-specific insertion plasmids, we synthesized a 1.1-kb fragment corresponding to the Hsp68 promoter and the *Peromyscus maniculatus Agouti* cDNA wildtype (WT) sequence by GenScript and then cloned these fragments into the PUC19 vector. From the WT template sequence, we deleted the Serine amino acid using a site-directed mutagenesis kit (New England Biolabs) to generate the ΔSer construct. Thus, the WT and ΔSer constructs are identical, except for the deletion of a single amino acid Serine at amino acid position 48. We digested the resulting vectors with ClaI and HindIII and then cloned these fragments into the pBT378.2 plasmid (Applied Stem Cell), which contains two AttB sites. We confirmed the plasmid sequences by Sanger sequencing.

Site-specific integration into H11P3 sites: The *Agouti* WT and ΔSer circular plasmids were individually mixed with *in vitro* transcribed φC31 integrase mRNA and microinjected by Applied Stem Cell into the pronuclei of heterozygous H11P3 embryos, harvested from C57BL/6 (B6) mice. In the presence of φC31 integrase, the attB sequences from the donor vector can undergo site-specific recombination with the attP sequences in the H11P3 mouse locus (*21*). We

transferred injected zygotes to the oviduct of CD1 foster mice and identified founder animals by PCR-based genotyping with primer pairs PR425N/*Agouti*-WT.v2-5GoI-R; *Agouti*-WT.v2-F2/*Agouti*-WT.v2-R2; *Agouti*-WT.v2-3GoI-F/Frt-R1 to screen for site-specific and random integrations (see figure S3 and table S9).

We then crossed founders containing site-specific insertions in the same orientation each to C57BL/6J mice to produce offspring in which we could characterize pigmentation phenotypes (as described above) and quantify the amount of pigment in hairs (see below).

Quantifying pheomelanin production

To measure the amount of pheomelanin in hairs, we homogenized hair samples (ca. 15 mg) with a Ten-Broeck glass homogenizer at a concentration of 10 mg/mL. We then subjected aliquots of 100 µL to hydroiodic acid hydrolysis (*22*) and alkaline hydrogen peroxide oxidation (*23*). We analyzed benzothiazine-type pheomelanin (BT-PM) as a specific degradation product of 4-amino-3-hydroxyphenylalanine (4-AHP) produced by the hydroiodic acid hydrolysis, while benzothiazole-type pheomelanin (BZ-PM) was quantified as thiazole-2,4,5-tricarboxylic acid (TTCA), produced by the alkaline hydrogen peroxide oxidation. Finally, we calculated the BT-PM and BZ-PM content by multiplying the 4-AHP and TTCA contents by factors of 7 and 34 respectively (*22*-*25*).

Measuring interactions between agouti and attractin using surface plasmon resonance

We used surface plasmon resonance (SPR) analysis on a BIAcore 3000 instrument to test for interactions between the agouti N-terminal WT and N-terminal ΔSer peptides with attractin ectodomain. Flow cells within a CM5 biosensor chip (GE Healthcare Life Sciences) were activated with N-hydroxysuccinimide (NHS) in the presence of 1-ethyl-3-(3-dimethylaminopropyl) carbodiimide hydrochloride generating an NHS ester that bound to free amines on full-length recombinant human Attractin ectodomain (*58*) passed over the surface (25 µg/ml in 100mM sodium acetate, pH 4.5). We blocked free NHS ester on the flowcell surface using ethanolamine (1 M). We next exposed an additional cell to immobilizing and blocking reagents in the absence of protein as a control surface. After extensive washing of the surfaces with binding buffer (10 mM HEPES, 150 mM NaCl, pH 7.0, 0.05% Tween 20), we assessed binding of the respective agouti peptides by injecting varying concentrations (0-312.5nM) simultaneously over the control and attractin surfaces. Note that the ectodomains of mouse and human Attractin share 94% identity, and full-length mouse agouti binds to human Attractin ectodomain with an apparent K_D of < 50nM. Between each cycle, we regenerated the surface using 20 mM glycine-HCl, pH 2.8. We corrected values shown in Resonance Units (RU) for non-specific binding by subtracting the SPR of the control flow chamber exposed to the same injected material followed by subtraction of buffer alone passing over the attractin surface. We analysed the resulting data using BIAevaluation 3.2 software and fitted the data to a 1:1 Langmuir binding model with separate k_d and k_a determinations. Finally, we calculated the dissociation constant (K_D) as k_d/k_a, and confirmed by manual linear transformation of the binding isotherms.

Genotyping the Serine deletion

To genotype all founding individuals for the ΔSer mutation, we designed a Custom TaqMan genotyping assay targeting WT and ΔSer *Agouti* sequences (*13*), using the TaqMan Custom Assay Design Tool (Thermo Fisher Scientific, Waltham, USA). We then used the resulting primers and probes with 2X TaqMan Genotyping Master Mix (Thermo Fisher Scientific),

following the manufacturer's protocol, to amplify and genotype samples in 96-well plates on a Mastercycler® RealPlex2 (Eppendorf, Hamburg, Germany).

Estimating selection on Serine deletion alleles and genotypes

To estimate the selection coefficient (*s*) for viability selection on the WT and ΔSer alleles in each replicate enclosure population, we calculated the change in frequency of each allele relative to the change in frequency of the WT allele, subtracted from 1, following (*59*). Similarly, *s* for genotypes was calculated as the change in frequency of the homozygous ΔSer genotype relative to the change in frequency of the homozygous WT genotype minus 1, when selection favored the homozygous ΔSer genotype. When there was evidence for selection against the homozygous ΔSer genotype, we calculated *s* as the change in frequency of the homozygous ΔSer genotype relative to the change in frequency of the homozygous WT genotype, subtracted from 1. This produces selection coefficients for the homozygous ΔSer genotype when it is favored and against the homozygous ΔSer genotype when it is selected against, using the homozygous WT genotype as the reference. We calculated *h* (the dominance coefficient) as the change in frequency of the heterozygous genotype subtracted from 1 divided by *s* of the homozygous ΔSer genotype (*59*). Standard errors for *s* and *h* are from measurements of $n = 3$ dark enclosures.

Supplementary Text

Application of the Wallenius' non-central hypergeometric distribution for modeling the enclosure experiment

For each polymorphic site S_i in the genotype data of the population we denote:

N: the number of valid genotypes at S_i
m: the vector of absolute genotype frequencies before predation at S_i, such that,

$N = \sum_{i=1}^{c} m_i$,for $m \in \{AA, Aa, aa\}$

,where c is the number of possible genotypes

n: the number of mice successively removed from the enclosure by predators

$\mathbf{x}_p$: the vector of absolute genotype frequencies in the predated individuals at S_i, such that,

$n = \mathbf{O}\, x_{2\%}$

$\mathbf{x}_s$: the vector of absolute genotype frequencies in the surviving individuals at S_i, such that,

$\boldsymbol{x}_4 = \boldsymbol{m} - \boldsymbol{x}_2$

w: the vector of weights for the three possible genotypes at S_i , where higher weights increase the chance of being predated.

The probability of observing a multivariate set $\mathbf{x}_p$, given **m** and **w** is given by the Wallenius' non-central hypergeometric distribution (*60*, *61*).

$$mwnchypg(\boldsymbol{x}_2; n, \boldsymbol{m}, \boldsymbol{w}) = \prod_{i=1}^{c} \binom{m_i}{x_i} \int_0^1 \prod_{i=1}^{c} (1 - t^{w_i/d})\, dt$$

,with $d = \sum_{i=1}^{c} w_i (m_i - x_i)$

Given $\mathbf{x}_p$ and **m** it is also possible to estimate **w** using the function "oddsWNCHypergeo" in the R package "BiasedUrn".

The distribution of genotype frequencies in the set of survivors at the end of the experiment is given by the complementary Wallenius' non-central distribution

$$mcwnchypg(\boldsymbol{x}_2; n, \boldsymbol{m}, \boldsymbol{w}) = mwnchypg(\boldsymbol{x}_4; N - n, \boldsymbol{m}, 1/w_1, \ldots, 1/w_c),\ w_i > 0.$$

We will refer to $1/w_i$ as the fitness of genotype *i*.

Constructing the null hypothesis that survival is independent of genotype at any locus

We can calculate for each variant, the probability that the distribution of genotype frequencies in the survivors is a random sample from the initial population. To do this we use the multivariate Wallenius non-central distribution with all weights set to 1. (In this special case, this distribution converges to the multivariate hypergeometric distribution).

$$p_{\mathrm{Z[\backslash]\hat{}\_`}} = mwnchypg\ (\boldsymbol{x}_4; N-n; \boldsymbol{m}, \boldsymbol{w}) :\ \boldsymbol{w} = (1,1,1)$$

For each polymorphic site, the elements of $\mathbf{x}_s$ ($x_{s,AA}$; $x_{s,Aa}$; $x_{s,aa}$) are calculated as:

$$x_{4,\mathrm{bb}} = \sum_{\%=(}^{f} \lambda_{\%} I_{\mathrm{bb}}(G_{\%}) \ , \lambda \in \{0,1\}$$

$$x_{4,\mathrm{b\_}} = \sum_{\%=(}^{f} \lambda_{\%} I_{\mathrm{b\_}}(G_{\%})$$

$$x_{4,\_} = N - x_{4,\mathrm{bb}} - x_{4,\mathrm{b\_}}$$

where λ is the survival vector such that $\lambda \epsilon \{0,1\}$ where 1 indicates survival, **G** is the vector of genotypes where **G** ϵ {AA, Aa, aa}, and I_{AA} is the indicator function such that $I_{AA}(G)$=1 if G="AA".

This is the probability represented in Figure 3A and B (using a log10 transformation). In this figure, variants are categorized into significant and non-significant variants based on an arbitrary significance threshold of α=0.01. We define Y_{obs} as the number of significant variants in a subset of the total number of variant S such that,

$$Y_{\mathrm{jk4}} = \sum_{\%=(}^{m} I_{4\%\mathbf{1Z}=p_{\mathrm{Z[\backslash]\hat{}\_`},\%@}} : \qquad I_{4\%\mathbf{1Z}}(p_{\mathrm{Z[\backslash]\hat{}\_`}}) := \begin{cases} 1\ if\ p_{\mathrm{Z[\backslash]\hat{}\_`}} \leq \alpha \\ 0\ if\ p_{\mathrm{Z[\backslash]\hat{}\_`}} > \alpha \end{cases}$$

we then approximate the expected distribution of Y under the assumption that survival is independent of genotype by randomly permuting the survival vector λ 1000 times and recalculating Y for each of the permutated dataset. We let $\mathbf{Y}_{neutral}$ be the vector containing the 1000 random values of Y and calculate the p-value of Y_{obs} as:

$$P(Y_{\mathrm{Z[\backslash]\hat{}\_`}} \geq Y_{\mathrm{jk4}}) = \frac{\sum_{\%=(}^{QQQ} I_{4\%\mathbf{1Zt}}(Y_{\mathrm{Z[\backslash]\hat{}\_`},\%})}{1000}$$

where,

$$I_{4\%\mathbf{1Zt}} := \begin{cases} 1\ if\ Y \geq Y_{\mathrm{jk4}} \\ 0\ if\ Y < Y_{\mathrm{jk4}} \end{cases}$$

Constructing the null hypothesis that survival depends only on a single locus under selection.

In the cases where Y_{obs} is significant, we further consider the possibility that survival can be affected by a single site under selection S_{sel}, where S_{sel} belongs to $\{1,2,\ldots,S_{max}\}$, the set of all variants in the dataset**.**

For each variant we calculate the fitness of each genotype using the multivariate Wallenius non-central distribution as explained above. We then obtain the selection and dominance coefficient *s* and *h* from the fitness values as

$s = \omega_{aa} - \omega_{AA}$
$h = (\omega_{Aa} - 1)/s$

We set ω_{aa} to be the highest fitness among homozygote genotypes such that *s* is always positive or equal to zero and, when possible, we report whether the *a* allele corresponds to the ancestral or derived state (*an outgroup sequence was available for Agouti, but not for the background loci*).

We then calculate the likelihood ratio statistic *D* as,

$$D = 2\ log\ S\frac{mwnchyp\{\boldsymbol{x}_4; N-n, \boldsymbol{m}, (\omega_{bb}, \omega_{b\_}, \omega_{\_\_})\}}{mwnchyp\{\boldsymbol{x}_s; N-n, \boldsymbol{m}, (1,1,1)\}}U$$

p-values for the test statistics are calculated under the assumption that *D* follows a chi-square distribution with 2 degrees of freedom.

We define S_{sel}, the site under selection, as the site associated with the smallest P value.

To test whether Y_{obs} is significant under the assumption that survival depends on genotype at locus S_{sel} we use the same resampling approach described above, but we sample the survivors according to the multivariate non-central Wallenius' distribution with the specific weights estimated for S_{sel}. This can be done with the function rMWNCHC() in the R package "BiasedUrn". (Null distributions shown in Figure 4C).

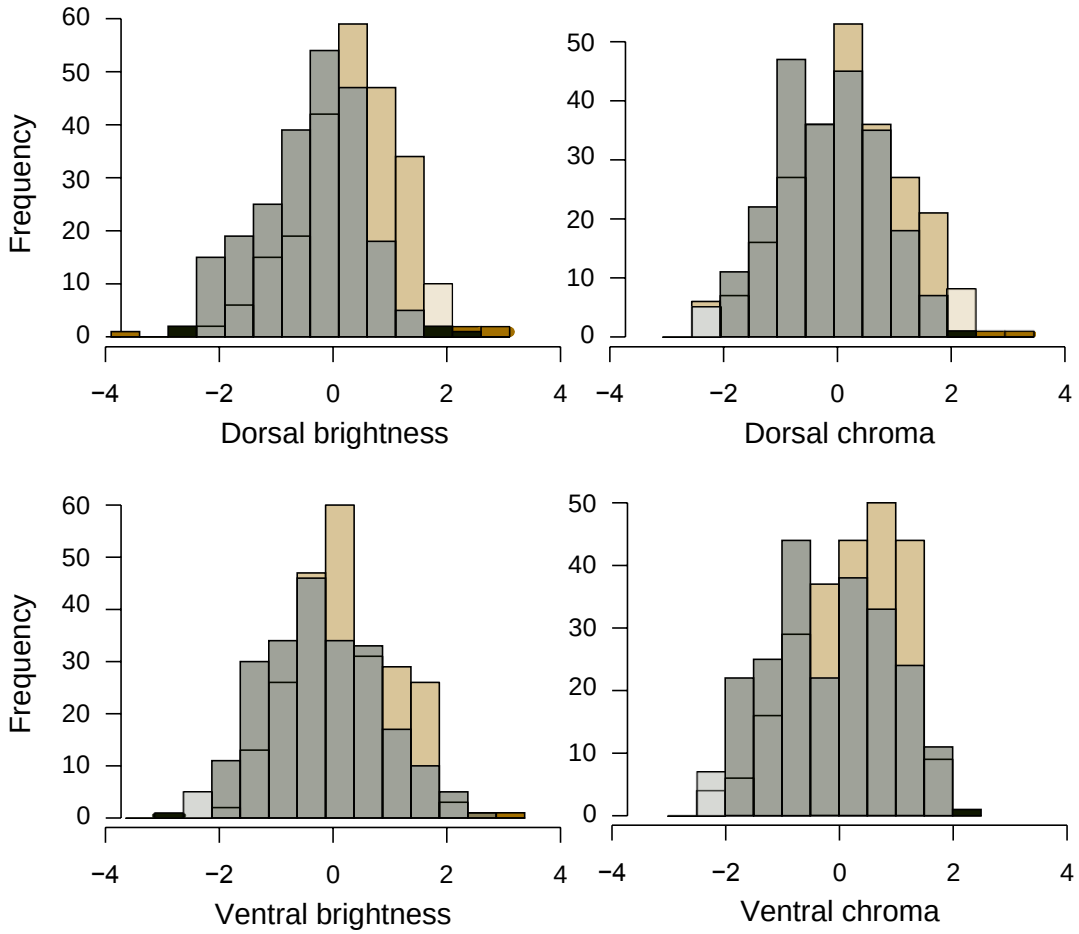

Figure S1. Distributions of quantitative pigmentation traits for mice captured on light (tan) versus dark (grey) habitat. Higher scores reflect lighter pigmentation (see Materials and Methods). All traits showed significant differences between mice captured on light versus dark habitat (two-sided t-tests, P <0.001).

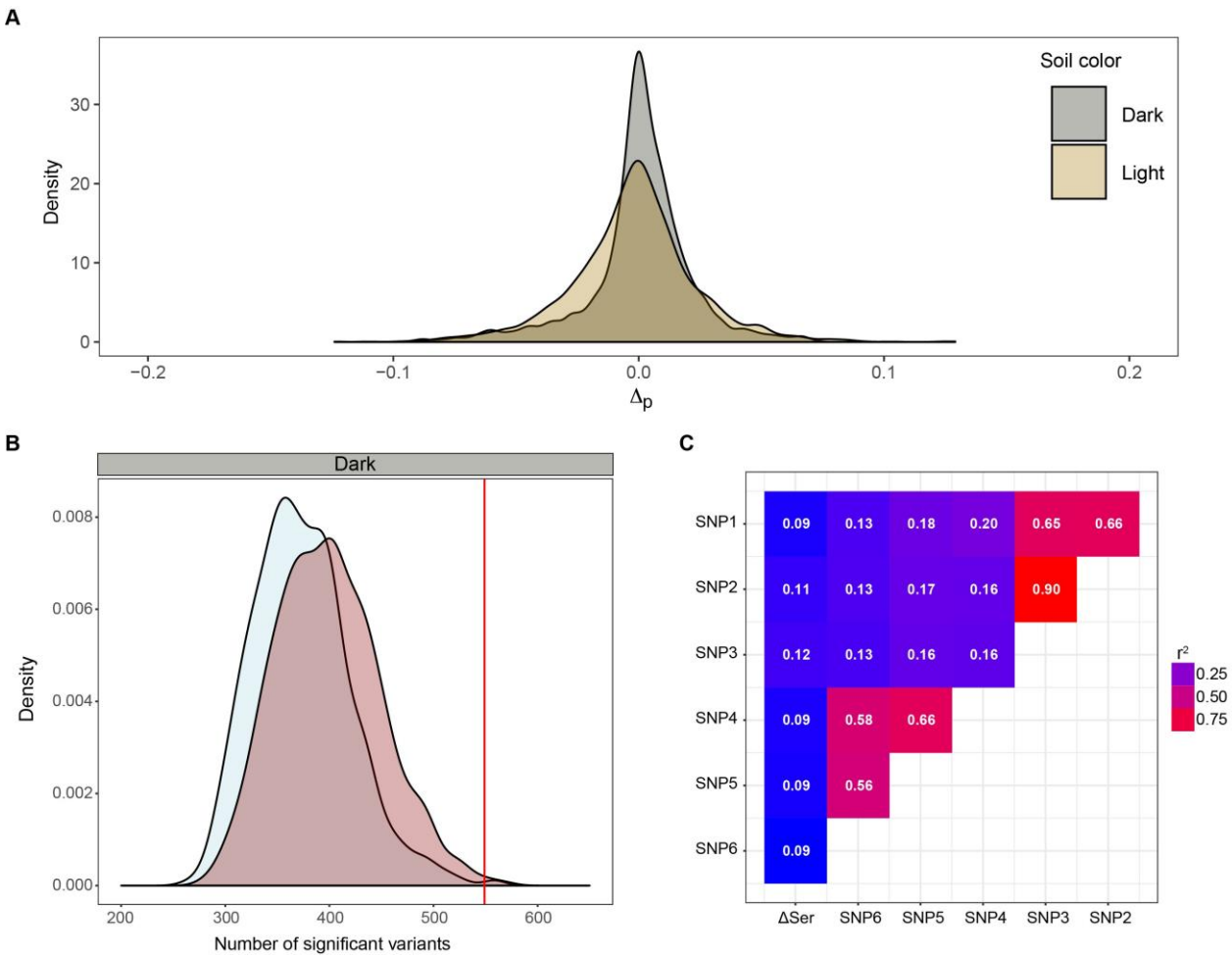

Figure S2. Allele frequency change and relationship between variants in *Agouti*. (**A**) Distribution of allele frequency changes at the *Agouti* locus in the light (tan) and dark (grey) enclosures (pooled). The larger frequency changes in light enclosures are consistent with the lower number of survivors and therefore higher sampling error. (**B**) Null distributions of the number of sites in *Agouti* expected to show significant allele frequency change at the 1% level in the dark enclosures. For the selection model, the site under selection is the site in the genome-wide control data with the lowest probability of having genotype frequencies in the survivors that are the result of random sampling. The observed number of significant sites is indicated by the vertical line. Note truncated x-axis. (**C**) Linkage disequilibrium (r^2) between the 7 candidate *Agouti* variants for selection listed in table S6.

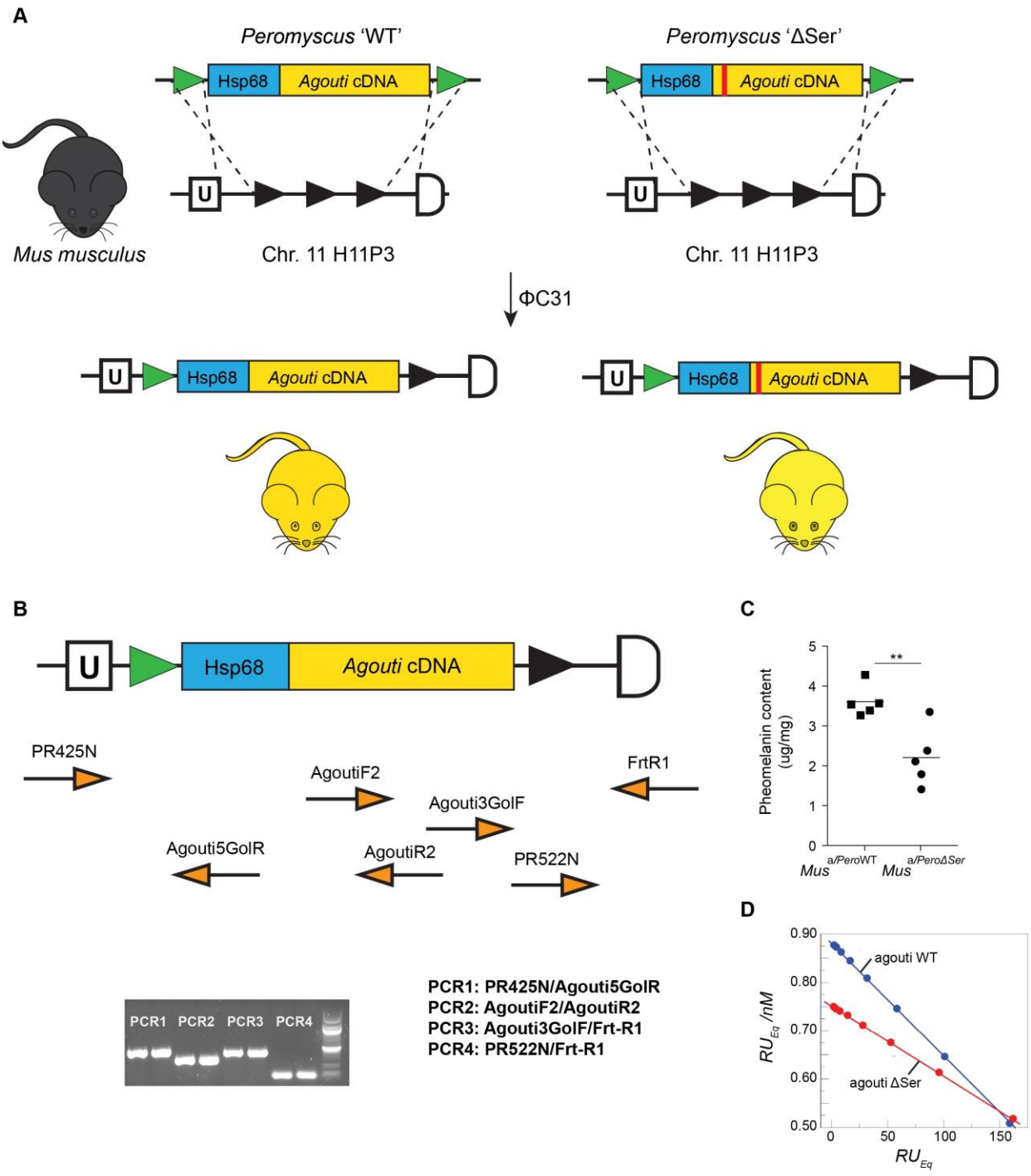

Fig S3. Functional experiments. (**A**)**,** In the presence of φC31 integrase, plasmids containing the Hsp68 promoter and the *Peromyscus Agouti* wildtype or ΔSer cDNA, as well as AttB, undergo site-specific recombination with the attP sequences of the H11P3 mouse locus and integrate into the genome. Founders have a mosaic black and yellow pattern but subsequent generations constitutively express agouti and have yellow coats. (**B**) Genotyping strategy used. See table S9 for primer sequences. (**C**) Pheomelanin degradation products (benzothiazole-type)

in the transgenic mice, measured with spectrophotometry and HPLC methods (ΔSer vs WT, two-tailed *t*-test; $n = 5$, $P = 0.006$). (**D**) Scatchard linear analysis was used to perform equilibrium binding analysis and determine the dissociation constant (K_d) for the interactions between the N-terminal domain of the *Peromyscus* wildtype (blue) or the ΔSer (red) agouti protein.

Table S1. Pair-wise correlation between pigment traits.

Trait 1	Trait 2	Slope	r^2	P value
Dorsal brightness	Dorsal chroma	-0.028	0.059	0.632
Dorsal brightness	Ventral brightness	0.030	0.054	0.576
Dorsal brightness	Ventral chroma	-0.015	0.053	0.779
Dorsal brightness	Tail pattern	-0.074	0.050	0.142
Dorsal chroma	Ventral brightness	0.002	0.050	0.965
Dorsal chroma	Ventral chroma	0.111	0.049	0.024*
Dorsal chroma	Tail pattern	-0.118	0.046	0.010*
Ventral brightness	Ventral chroma	0.055	0.054	0.307
Ventral brightness	Tail pattern	-0.108	0.051	0.034*
Ventral chroma	Tail pattern	-0.074	0.051	0.153

* = P<0.05, F-test

Table S2. Model coefficients and 95% BCI for the interaction effect between predictor variables and experimental treatment.

Variable	Mean	2.5% BCI	97.5% BCI
Source habitat	1.352	0.695	1.984
Dorsal brightness	0.751	0.382	1.113
Dorsal chroma	0.023	-0.291	0.341
Ventral brightness	0.164	-0.172	0.500
Ventral chroma	0.005	-0.325	0.344

Estimates and Bayesian Credible Intervals (BCI) obtained from a Cormack-Jolly-Seber capture-recapture model (*18*). Models containing each predictor were run separately.

Table S3. Standardized linear selection gradients (β) for pigmentation traits.

Trait	Dark site			Light site		
	Enclosure 1	Enclosure 2	Enclosure 3	Enclosure 1	Enclosure 2	Enclosure 3
Dorsal brightness	-0.212 (0.289)	-0.411** (0.151)	-0.385** (0.156)	1.115* (0.830)	0.649** (0.140)	0.561 (0.463)
Dorsal chroma	-0.083 (0.156)	0.250 (0.137)	0.034 (0.124)	-0.214 (0.362)	0.069 (0.211)	-0.321 (0.372)
Ventral brightness	-0.151 (0.149)	0.027 (0.128)	-0.133 (0.129)	0.246 (0.577)	-0.102 (0.183)	-0.562 (0.772)
Ventral chroma	-0.114 (0.154)	-0.097 (0.144)	0.300** (0.105)	-0.019 (0.487)	-0.229 (0.163)	0.133 (0.352)
Tail pattern	-0.006 (0.183)	-0.133 (0.144)	0.081 (0.135)	-0.139 (0.721)	0.343 (0.176)	0.385 (0.478)

Parentheses give 1 standard error. Standard errors and P values determined by 1000 bootstrap replicates. All selection gradients calculated over the first 3 months following introduction to the enclosures. *: $P < 0.05$, **: $P < 0.005$.

Table S4. Standardized quadratic selection gradients (ϒ) for pigmentation traits.

Trait	Dark site			Light site		
	Enclosure 1	Enclosure 2	Enclosure 3	Enclosure 1	Enclosure 2	Enclosure 3
Dorsal brightness	-0.037 (0.534)	0.021 (0.051)	-0.005 (0.077)	1.013 (3.985)	0.202 (0.162)	0.143 (0.467)
Dorsal chroma	-0.006 (0.065)	0.008 (0.022)	0.000 (0.010)	0.037 (0.727)	0.002 (0.047)	0.047 (0.269)
Ventral brightness	-0.019 (0.748)	0.000 (0.007)	-0.001 (0.013)	0.050 (0.642)	0.005 (0.038)	0.144 (1.297)
Ventral chroma	-0.011 (0.413)	0.001 (0.014)	-0.003 (0.034)	0.000 (0.754)	0.025 (0.052)	0.008 (0.116)
Tail pattern	0.000 (0.574)	0.002 (0.014)	0.000 (0.017)	0.016 (199.713)	0.057 (0.097)	0.067 (0.436)

Parentheses give 1 standard error. Standard errors and P values determined by 1000 bootstrap replicates. All selection gradients calculated over the first three months following introduction to the enclosures. $P > 0.05$ in all cases.

Table S5. Standardized quadratic selection gradients (ϒ) for correlational selection on pigmentation traits.

Traits	Dark site			Light site		
	Enclosure 1	Enclosure 2	Enclosure 3	Enclosure 1	Enclosure 2	Enclosure 3
Dorsal brightness * Dorsal chroma	-0.015 (0.130)	-0.013 (0.026)	0.000 (0.019)	-0.194 (1.518)	0.021 (0.083)	-0.082 (0.208)
Dorsal brightness * Ventral brightness	-0.026 (0.303)	-0.001 (0.014)	-0.002 (0.019)	0.224 (1.243)	-0.032 (0.078)	-0.144 (0.668)
Dorsal brightness * Ventral chroma	-0.010 (0.106)	0.001 (0.008)	0.000 (0.007)	-0.043 (0.518)	-0.003 (0.029)	0.082 (0.343)
Dorsal brightness * Tail stripe	-0.020 (0.247)	0.005 (0.017)	0.004 (0.037)	-0.018 (1.445)	-0.071 (0.071)	0.034 (0.142)
Dorsal chroma * Ventral brightness	-0.008 (0.085)	-0.003 (0.011)	0.000 (0.013)	0.003 (0.663)	-0.008 (0.032)	-0.019 (0.108)
Dorsal chroma * Ventral chroma	-0.014 (0.552)	0.000 (0.007)	0.001 (0.017)	-0.004 (0.526)	0.011 (0.034)	-0.034 (0.190)
Dorsal chroma * Tail stripe	-0.001 (0.256)	0.007 (0.023)	0.001 (0.020)	-0.126 (8.618)	0.107 (0.112)	0.098 (0.394)
Ventral brightness * Ventral chroma	0.000 (0.061)	-0.004 (0.012)	0.000 (0.008)	0.024 (3.308)	0.011 (0.061)	-0.056 (0.189)

Ventral brightness * Tail stripe	-0.001 (0.128)	0.000 (0.006)	0.000 (0.011)	-0.028 (6.627)	-0.017 (0.045)	-0.098 (0.595)
Ventral chroma * Tail stripe	-0.001 (0.107)	0.002 (0.008)	-0.001 (0.017)	0.002 (4.4375)	-0.038 (0.044)	0.023 (0.157)

Parentheses give 1 standard error. Standard errors and p-values determined by 1000 bootstrap replicates. All selection gradients calculated over the first three months following introduction to the enclosures. $P > 0.05$ in all cases.

Table S6. Candidate SNPs for targets of direct selection.

Variant	Chromosome	Position	Initial frequency	Frequency change[1]	PIP[2]	LRT	P value[3]	P value[4]	F_{st}[5]
SNP1	chr4	131439350	0.43	-0.08	0.16	11.54	0.02	0.11	0.20
SNP2	chr4	131442316	0.39	-0.09	0.16	15.89	0.01	0.06	0.18
SNP3	chr4	131442394	0.39	-0.09	0.11	17.43	0.01	0.05	0.20
SNP4	chr4	131471739	0.28	-0.06	0.12	9.84	0.03	0.14	0.08
SNP5	chr4	131471821	0.31	-0.07	0.21	11.11	0.02	0.11	0.10
SNP6	chr4	131472069	0.31	-0.08	0.12	13.25	0.01	0.10	0.13
ΔSer	chr4	131474564	0.26	-0.06	0.54	10.67	0.02	0.12	0.34

1: Mean allele frequency change in the dark enclosures
2: Posterior inclusion probability (PIP) indicating the strength of the association with dorsal brightness
3: FDR-corrected P value of the LRT test when considering only variants in *Agouti* with a MAF >10% and associated with dorsal brightness
4: FDR-corrected P value of the LRT test when considering all variants in *Agouti* with a MAF >10%
5: Weir and Cockerham F_{st} between mice captured in light versus dark habitat

Table S7. Relative fitness of Serine deletion genotypes and alleles.

	Dark site			Light site		
	Enclosure 1	Enclosure 2	Enclosure 3	Enclosure 1	Enclosure 2	Enclosure 3
Genotype						
ΔSer/ΔSer	0.166	0.344	0.861	1.500	0.825	1.271
ΔSer/WT	0.870	0.891	0.833	0.667	1.050	0.763
WT/WT	1	1	1	1	1	1
Allele						
ΔSer	0.873	0.673	0.502	1.046	0.949	1.074
WT	1	1	1	1	1	1

Table S8. Sampling locations of mice.

Location	Full name	Habitat type	Coordinates
MER	Merritt Reservoir	Light	42 35'42" 105 55'09"
BILL	Bill's field	Dark	42 54'05" 100 30'32"
DAN	Danielski's field	Dark	42 50'48" 100 34'01"
SCH	Schlagel creek	Light	42 42'07" 100 37'00"
SMF	Samuel McKelvie National Forest	Light	42 39'09" 100 56'37"
LON	Lonnie's field	Dark	42 54'34" 100 34'37"

Table S9. Primers used for genotyping the transgenic *Mus* lines.

PR425N	GGTGATAGGTGGCAAGTGGTATTCCGTAAG-
Agouti5GoIR	CGGCTGCTCAGTTTGGATGTTC
AgoutiF2	AGGAGACGCTCAGAGATGACAAG
AgoutiR2	GTTAGGGTTGAGTACGCGGCAG
Agouti3GoIF	CGCGTACTCAACCCTAACTGC
PR522N	GACGATGTAGGTCACGGTCTCGAAG
Frt-R1	GGAATAGGAACTTCGTCGACA

References and Notes

1. R. Mallarino, C. Henegar, M. Mirasierra, M. Manceau, C. Schradin, M. Vallejo, S. Beronja, G. S. Barsh, H. E. Hoekstra, Developmental mechanisms of stripe patterns in rodents. *Nature* **539**, 518–523 (2016). doi:10.1038/nature20109 Medline

2. M. A. Ilardo, I. Moltke, T. S. Korneliussen, J. Cheng, A. J. Stern, F. Racimo, P. de Barros Damgaard, M. Sikora, A. Seguin-Orlando, S. Rasmussen, I. C. L. van den Munckhof, R. Ter Horst, L. A. B. Joosten, M. G. Netea, S. Salingkat, R. Nielsen, E. Willerslev, Physiological and genetic adaptations to diving in sea nomads. *Cell* **173**, 569–580.e15 (2018). doi:10.1016/j.cell.2018.03.054 Medline

3. D. Bradley, P. Xu, I.-I. Mohorianu, A. Whibley, D. Field, H. Tavares, M. Couchman, L. Copsey, R. Carpenter, M. Li, Q. Li, Y. Xue, T. Dalmay, E. Coen, Evolution of flower color pattern through selection on regulatory small RNAs. *Science* **358**, 925–928 (2017). doi:10.1126/science.aao3526 Medline

4. J. G. Kingsolver, S. E. Diamond, A. M. Siepielski, S. M. Carlson, Synthetic analyses of phenotypic selection in natural populations: Lessons, limitations and future directions. *Evol. Ecol.* **26**, 1101–1118 (2012). doi:10.1007/s10682-012-9563-5

5. O. Lapiedra, T. W. Schoener, M. Leal, J. B. Losos, J. J. Kolbe, Predator-driven natural selection on risk-taking behavior in anole lizards. *Science* **360**, 1017–1020 (2018). doi:10.1126/science.aap9289 Medline

6. S. K. Auer, C. A. Dick, N. B. Metcalfe, D. N. Reznick, Metabolic rate evolves rapidly and in parallel with the pace of life history. *Nat. Commun.* **9**, 14 (2018). doi:10.1038/s41467-017-02514-z Medline

7. R. A. Bay, N. Rose, R. Barrett, L. Bernatchez, C. K. Ghalambor, J. R. Lasky, R. B. Brem, S. R. Palumbi, P. Ralph, Predicting responses to contemporary environmental change using evolutionary response architectures. *Am. Nat.* **189**, 463–473 (2017). doi:10.1086/691233 Medline

8. R. D. Barrett, H. E. Hoekstra, Molecular spandrels: Tests of adaptation at the genetic level. *Nat. Rev. Genet.* **12**, 767–780 (2011). doi:10.1038/nrg3015 Medline

9. D. B. Loope, J. Swinehart, Thinking like a dune field: Geologic history in the Nebraska Sand Hills. *Great Plains Res.* **10**, 5–35 (2000).

10. A. Bleed, *Atlas of the Sand Hills* (University of Nebraska, Omaha, 1990).

11. L. R. Dice, Variation of the deer-mouse (*Peromyscus maniculatus*) on the Sand Hills of Nebraska and adjacent areas. *Contributions from the Laboratory of Vertebrate Genetics*. *University of Michigan* **15**, 1–19 (1941).

12. L. Dice, Effectiveness of selection by owls of deer mice (*Peromyscus maniculatus*) which contrast in color with their background. *Contributions from the Laboratory of Vertebrate Biology*. *University of Michigan* **34**, 1–20 (1947).

13. C. R. Linnen, E. P. Kingsley, J. D. Jensen, H. E. Hoekstra, On the origin and spread of an adaptive allele in deer mice. *Science* **325**, 1095–1098 (2009). doi:10.1126/science.1175826 Medline

14. C. R. Linnen, Y.-P. Poh, B. K. Peterson, R. D. H. Barrett, J. G. Larson, J. D. Jensen, H. E. Hoekstra, Adaptive evolution of multiple traits through multiple mutations at a single gene. *Science* **339**, 1312–1316 (2013). doi:10.1126/science.1233213 Medline

15. S. P. Pfeifer, S. Laurent, V. C. Sousa, C. R. Linnen, M. Foll, L. Excoffier, H. E. Hoekstra, J. D. Jensen, The evolutionary history of Nebraska deer mice: Local adaptation in the face of strong gene flow. *Mol. Biol. Evol.* **35**, 792–806 (2018). doi:10.1093/molbev/msy004 Medline

16. M. Manceau, V. S. Domingues, C. R. Linnen, E. B. Rosenblum, H. E. Hoekstra, Convergence in pigmentation at multiple levels: Mutations, genes and function. *Philos. Trans. R. Soc. Lond. B Biol. Sci.* **365**, 2439–2450 (2010). doi:10.1098/rstb.2010.0104 Medline

17. Y. Chen, D. M. J. Duhl, G. S. Barsh, Opposite orientations of an inverted duplication and allelic variation at the mouse agouti locus. *Genetics* **144**, 265–277 (1996). Medline

18. See supplementary materials.

19. R. H. Baker, *Michigan Mammals* (Wayne State Univ., Detroit, 1983).

20. V. S. Domingues, Y.-P. Poh, B. K. Peterson, P. S. Pennings, J. D. Jensen, H. E. Hoekstra, Evidence of adaptation from ancestral variation in young populations of beach mice. *Evolution* **66**, 3209–3223 (2012). doi:10.1111/j.1558-5646.2012.01669.x Medline

21. B. Tasic, S. Hippenmeyer, C. Wang, M. Gamboa, H. Zong, Y. Chen-Tsai, L. Luo, Site-specific integrase-mediated transgenesis in mice via pronuclear injection. *Proc. Natl. Acad. Sci. U.S.A.* **108**, 7902–7907 (2011). doi:10.1073/pnas.1019507108 Medline

22. K. Wakamatsu, S. Ito, J. L. Rees, The usefulness of 4-amino-3-hydroxyphenylalanine as a specific marker of pheomelanin. *Pigment Cell Res.* **15**, 225–232 (2002). doi:10.1034/j.1600-0749.2002.02009.x Medline

23. S. Ito, Y. Nakanishi, R. K. Valenzuela, M. H. Brilliant, L. Kolbe, K. Wakamatsu, Usefulness of alkaline hydrogen peroxide oxidation to analyze eumelanin and pheomelanin in various tissue samples: Application to chemical analysis of human hair melanins. *Pigment Cell Melanoma Res.* **24**, 605–613 (2011). doi:10.1111/j.1755-148X.2011.00864.x Medline

24. M. d'Ischia, K. Wakamatsu, A. Napolitano, S. Briganti, J.-C. Garcia-Borron, D. Kovacs, P. Meredith, A. Pezzella, M. Picardo, T. Sarna, J. D. Simon, S. Ito, Melanins and melanogenesis: Methods, standards, protocols. *Pigment Cell Melanoma Res.* **26**, 616–633 (2013). doi:10.1111/pcmr.12121 Medline

25. S. Del Bino, S. Ito, J. Sok, Y. Nakanishi, P. Bastien, K. Wakamatsu, F. Bernerd, Chemical analysis of constitutive pigmentation of human epidermis reveals constant eumelanin to pheomelanin ratio. *Pigment Cell Melanoma Res.* **28**, 707–717 (2015). doi:10.1111/pcmr.12410 Medline

26. L. He, T. M. Gunn, D. M. Bouley, X.-Y. Lu, S. J. Watson, S. F. Schlossman, J. S. Duke-Cohan, G. S. Barsh, A biochemical function for attractin in agouti-induced pigmentation and obesity. *Nat. Genet.* **27**, 40–47 (2001). doi:10.1038/83741 Medline

27. P. R. Grant, B. R. Grant, Predicting microevolutionary responses to directional selection on heritable variation. *Evolution* **49**, 241–251 (1995). doi:10.1111/j.1558-5646.1995.tb02236.x Medline

28. P. Nosil, R. Villoutreix, C. F. de Carvalho, T. E. Farkas, V. Soria-Carrasco, J. L. Feder, B. J. Crespi, Z. Gompert, Natural selection and the predictability of evolution in *Timema* stick insects. *Science* **359**, 765–770 (2018). doi:10.1126/science.aap9125 Medline

29. M. Bosse, L. G. Spurgin, V. N. Laine, E. F. Cole, J. A. Firth, P. Gienapp, A. G. Gosler, K. McMahon, J. Poissant, I. Verhagen, M. A. M. Groenen, K. van Oers, B. C. Sheldon, M. E. Visser, J. Slate, Recent natural selection causes adaptive evolution of an avian polygenic trait. *Science* **358**, 365–368 (2017). doi:10.1126/science.aal3298 Medline

30. R. Fisher, *The Genetical Theory of Natural Selection* (Oxford Univ. Press, 1930).

31. R. Bürger, M. Lynch, Evolution and extinction in a changing environment: A quantitative-genetic analysis. *Evolution* **49**, 151–163 (1995). doi:10.1111/j.1558-5646.1995.tb05967.x Medline

32. J. G. Kingsolver, H. E. Hoekstra, J. M. Hoekstra, D. Berrigan, S. N. Vignieri, C. E. Hill, A. Hoang, P. Gibert, P. Beerli, The strength of phenotypic selection in natural populations. *Am. Nat.* **157**, 245–261 (2001). doi:10.1086/319193 Medline

33. A. M. Siepielski, J. D. DiBattista, S. M. Carlson, It's about time: The temporal dynamics of phenotypic selection in the wild. *Ecol. Lett.* **12**, 1261–1276 (2009). doi:10.1111/j.1461-0248.2009.01381.x Medline

34. A. M. Siepielski, K. M. Gotanda, M. B. Morrissey, S. E. Diamond, J. D. DiBattista, S. M. Carlson, The spatial patterns of directional phenotypic selection. *Ecol. Lett.* **16**, 1382–1392 (2013). doi:10.1111/ele.12174 Medline

35. M. Nei, Y. Suzuki, M. Nozawa, The neutral theory of molecular evolution in the genomic era. *Annu. Rev. Genomics Hum. Genet.* **11**, 265–289 (2010). doi:10.1146/annurev-genom-082908-150129 Medline

36. R. Nielsen, Molecular signatures of natural selection. *Annu. Rev. Genet.* **39**, 197–218 (2005). doi:10.1146/annurev.genet.39.073003.112420 Medline

37. J. D. Jensen, M. Foll, L. Bernatchez, The past, present and future of genomic scans for selection. *Mol. Ecol.* **25**, 1–4 (2016). doi:10.1111/mec.13493 Medline

38. T. J. Thurman, R. D. H. Barrett, The genetic consequences of selection in natural populations. *Mol. Ecol.* **25**, 1429–1448 (2016). doi:10.1111/mec.13559 Medline

39. P. Librado, C. Der Sarkissian, L. Ermini, M. Schubert, H. Jónsson, A. Albrechtsen, M. Fumagalli, M. A. Yang, C. Gamba, A. Seguin-Orlando, C. D. Mortensen, B. Petersen, C. A. Hoover, B. Lorente-Galdos, A. Nedoluzhko, E. Boulygina, S. Tsygankova, M. Neuditschko, V. Jagannathan, C. Thèves, A. H. Alfarhan, S. A. Alquraishi, K. A. S. Al-Rasheid, T. Sicheritz-Ponten, R. Popov, S. Grigoriev, A. N. Alekseev, E. M. Rubin, M. McCue, S. Rieder, T. Leeb, A. Tikhonov, E. Crubézy, M. Slatkin, T. Marques-Bonet, R. Nielsen, E. Willerslev, J. Kantanen, E. Prokhortchouk, L. Orlando, Tracking the origins of Yakutian horses and the genetic basis for their fast adaptation to subarctic

environments. *Proc. Natl. Acad. Sci. U.S.A.* **112**, E6889–E6897 (2015). doi:10.1073/pnas.1513696112 Medline

40. Y. Kim, D. Gulisija, Signatures of recent directional selection under different models of population expansion during colonization of new selective environments. *Genetics* **184**, 571–585 (2010). doi:10.1534/genetics.109.109447 Medline

41. G. S. Bradburd, P. L. Ralph, G. M. Coop, Disentangling the effects of geographic and ecological isolation on genetic differentiation. *Evolution* **67**, 3258–3273 (2013). doi:10.1111/evo.12193 Medline

42. S. Peischl, I. Dupanloup, A. Foucal, M. Jomphe, V. Bruat, J.-C. Grenier, A. Gouy, K. J. Gilbert, E. Gbeha, L. Bosshard, E. Hip-Ki, M. Agbessi, A. Hodgkinson, H. Vézina, P. Awadalla, L. Excoffier, Relaxed selection during a recent human expansion. *Genetics* **208**, 763–777 (2018). doi:10.1534/genetics.117.300551 Medline

43. A. P. Hendry, *Eco-evolutionary dynamics* (Princeton Univ. Press, Princeton, 2017).

44. R. D. H. Barrett, S. Laurent, R. Mallarino, S. P. P, C. C. Y. Xu, M. Foll, K. Wakamatsu, J. S. Duke-Cohan, J. D. Jensen, H. E. Hoekstra, Data from: Linking a mutation to survival in wild mice, Dryad Digital Repository (2018). doi:10.5061/dryad.60mk699.

45. R. D. H. Barrett, L. K. M'Gonigle, mouse-recapture-v1.0.0, Version 1.0.0, Zenodo (2018). doi:10.5281/zenodo.1758243.

46. S. Badion, S. Laurent, rsurvival-0.1.0, Version 0.1.0, Zenodo (2018). doi:10.5281/zenodo.1753895.

47. J. Botten, R. Nofchissey, H. Kirkendoll-Ahern, P. Rodriguez-Moran, I. A. Wortman, D. Goade, T. Yates, B. Hjelle, Outdoor facility for quarantine of wild rodents infected with hantavirus. *J. Mammal.* **81**, 250–259 (2000). doi:10.1644/1545-1542(2000)081<0250:OFFQOW>2.0.CO;2

48. R. Montgomerie, CLR, version 1.05 (2008); http://post.queensu.ca/~mont/color/analyze.html

49. B. Tabachnick, L. S. Fidell, *Using Multivariate Statistics* (Allyn and Bacon, Boston, ed. 4, 2001).

50. H. E. Hoekstra, R. J. Hirschmann, R. A. Bundey, P. A. Insel, J. P. Crossland, A single amino acid mutation contributes to adaptive beach mouse color pattern. *Science* **313**, 101–104 (2006). doi:10.1126/science.1126121 Medline

51. J.-D. Lebreton, K. P. Burnham, J. Clobert, D. R. Anderson, Modeling survival and testing biological hypotheses using marked animals: A unified approach with case studies. *Ecol. Monogr.* **62**, 67–118 (1992). doi:10.2307/2937171

52. S. Pledger, K. H. Pollock, J. L. Norris, Open capture-recapture models with heterogeneity: I. Cormack-Jolly-Seber model. *Biometrics* **59**, 786–794 (2003). doi:10.1111/j.0006-341X.2003.00092.x Medline

53. M. Kery, M. Schaub, *Bayesian Population Analysis Using WinBUGS: A Hierarchical Perspective* (Academic Press, 2011).

54. R. Lande, S. J. Arnold, The measurement of selection on correlated characters. *Evolution* **37**, 1210–1226 (1983). doi:10.1111/j.1558-5646.1983.tb00236.x Medline

55. D. Schluter, Estimating the form of natural selection on a quantitative trait. *Evolution* **42**, 849–861 (1988). doi:10.1111/j.1558-5646.1988.tb02507.x Medline

56. M. B. Morrissey, K. Sakrejda, Unification of regression-based methods for the analysis of natural selection. *Evolution* **67**, 2094–2100 (2013). doi:10.1111/evo.12077 Medline

57. S. N. Wood, Fast stable restricted maximum likelihood and marginal likelihood estimation of semiparametric generalized linear models. *J. R. Stat. Soc. Series B Stat. Methodol.* **73**, 3–36 (2011). doi:10.1111/j.1467-9868.2010.00749.x

58. D. Schluter, D. Nychka, Exploring fitness surfaces. *Am. Nat.* **143**, 597–616 (1994). doi:10.1086/285622

59. E. P. Kingsley, M. Manceau, C. D. Wiley, H. E. Hoekstra, Melanism in *peromyscus* is caused by independent mutations in *agouti*. *Public Library of Science One* **4**, e6435 (2009). Medline

60. T. Magoč, S. L. Salzberg, FLASH: Fast length adjustment of short reads to improve genome assemblies. *Bioinformatics* **27**, 2957–2963 (2011). doi:10.1093/bioinformatics/btr507 Medline

61. W. Tang, T. M. Gunn, D. F. McLaughlin, G. S. Barsh, S. F. Schlossman, J. S. Duke-Cohan, Secreted and membrane attractin result from alternative splicing of the human ATRN gene. *Proc. Natl. Acad. Sci. U.S.A.* **97**, 6025–6030 (2000). doi:10.1073/pnas.110139897 Medline

62. D. Hartl, A. Clark, *Principles of Population Genetics* (Sinauer Associates, Sunderland, 1997).

63. J. Chesson, A non-central multivariate hypergeometric distribution arising from biased sampling with application to selective predation. *J. Appl. Probab.* **13**, 795–797 (1976). doi:10.2307/3212535

64. A. Fog, Sampling methods for Wallenius' and Fisher's noncentral hypergeometric distributions. *Commun. Stat. Simul. Comput.* **37**, 241–257 (2008). doi:10.1080/03610910701790236